Strain dependence of dissociative adsorption of H_2O on epitaxially strained, out-of-plane polarized, $BaTiO_3$(001) thin films

J.L. Wang [a,b], S.J. She [a], F. Gaillard [c], G. Niu [d], B. Vilquin [e], N. Barrett [f,*]

[a] College of Science, Donghua University, Shanghai 201620, China
[b] Shanghai Institute of Intelligent Electronics and Systems, Donghua University, Shanghai 201620, China
[c] Univ Lyon, Université Claude Bernard Lyon 1, CNRS, IRCELYON-UMR 5256, Villeurbanne cedex 69626, France
[d] Electronic Materials Research Laboratory, Key Laboratory of the Ministry of Education and International Center for Dielectric Research, School of Electronic and Information Engineering, Xi'an Jiaotong University, Xi'an 710049, China
[e] Université de Lyon, Ecole Centrale de Lyon, Institut des Nanotechnologies de Lyon, Ecully cedex F- 69134, France
[f] SPEC, CEA, CNRS, Université Paris Saclay, Gif-sur-Yvette F-91191, France

ARTICLE INFO

ABSTRACT

The strain dependence of the apparent activation energy of desorption of H_2O on epitaxial, TiO_2-terminated, out-of-plane polarized, $BaTiO_3$(100) thin films has been investigated using X-ray diffraction, X-ray photoelectron spectroscopy and temperature-programmed desorption. The apparent activation energy of desorption increases significantly with the in-plane strain, suggesting that the strain-induced ferroelectric distortion determines the strength of the chemical bond between the dissociatively adsorbed water and the surface.

1. Introduction

Strain and polarization are closely linked in ferroelectrics. In the typical perovskite oxide ferroelectric $BaTiO_3$ the bulk ferroelectric tetragonal phase shows an in-plane distortion of 0.2% with respect to the centrosymmetric cubic phase. Increasing the distortion increases the tetragonality and therefore the Ti off-centering, leading to stronger polarization. High-quality, epitaxial growth can be used to impose strains an order of magnitude greater than those possible in bulk crystals enhancing the film polarization. On the other hand, ferroelectric surfaces are also very reactive and stronger polarization will enhance the reactivity with for example, ambient water, significantly modifying the surface properties.

Water can exist at the surface in molecular form or dissociate into hydroxyl (OH^-) groups and protons (H^+). As they are both polar entities, they can interact with the polarity at the surface of a ferroelectric material to form a particular electrical boundary condition and influence the polarization [1]. OH^- groups can fill lattice oxygen vacancies (V_O) or form on-top chemical bonds with surface cations while H^+ can bond to lattice oxygen. Indeed, the presence of hydrogen in ferroelectrics is known as a leading factor in imprint effects [2]. The tetragonal distortion determines the polarization, therefore, the interaction of an out of plane polarized surface should also vary with strain. In this article, we investigate the influence of the tetragonal distortion in epitaxially strained, out of plane polarized $BaTiO_3$ (BTO) thin films on the strength of the chemisorption sites and the apparent activation energy of desorption (E_{app}).

Previously, we studied the chemisorption sites of water on fully strained 8 nm $BaTiO_3$ films with varying V_O concentration and showed that OH^- groups can either fill surface V_O or on-top bond to surface cations [3]. Here we have tuned the in-plane strain by varying the film thickness from 8 (fully strained) to 30 nm (fully relaxed) to probe the influence on the apparent activation energy of desorption.

We have used X-ray diffraction (XRD) to characterize the strain of the BTO films as a function of thickness. Then, X-ray photoelectron spectroscopy (XPS) is used to characterize the number and type of adsorption sites. Finally, thermally programmed desorption (TPD) allows to extract the apparent activation energy of desorption (E_{app}). The results confirm the presence of OH^- groups chemically bonded on-top of surface Ti atoms and probably to Ba atoms at step edges. They show that E_{app} of water decreases with increasing of film thickness and is correlated with the strain-induced polar distortion.

---

* Corresponding author.
  E-mail address: nick.barrett@cea.fr (N. Barrett).

2. Experiment

A TiO$_2$-terminated SrTiO$_3$ (001) surface composed of single unit cell steps and atomically flat terraces was prepared following the established protocol using a commercial substrate [4]. After heating the substrate to 650 °C for 1 h under an oxygen partial pressure of $\sim 10^{-4}$ Pa to remove carbon contamination on the surface, 8, 15 and 30 nm TiO$_2$-terminated BTO films were grown by molecular beam epitaxy with a growth rate of ~ 1 ML/min as previously described [3]. The unique TiO$_2$ surface termination is confirmed by the integral number off RHEED oscillations observed during growth and the systematic unit cell step height observed by Atomic Force Microscopy [3]. Before XPS analysis, the films were heated to remove any surface contamination resulting from sample transfer in air but the annealing temperature of 600 °C was below that used in the molecular beam epitaxy growth, making unlikely any possible surface phase separation.

The in and out of plane lattice constants were determined from XRD using a high-resolution x-ray diffraction (six-circle Rigaku SmartLab diffractometer with rotating anode using Cu Kα_I line, $\lambda = 1.5406$ Å). Water exposure was performed in a dedicated ultra-high vacuum chamber. Pure H$_2$O was obtained by freeze-pump-thaw cycles and then introduced at 1×10^{-2} Pa for 1 h, equal to 4.7×10^5 langmuir. After exposure, samples were transferred under vacuum to the analysis chamber for the XPS measurements.

XPS was carried out using a hemispherical analyzer with a 128-channel strip anode detector and a monochromatic Al Kα (1486.7 eV) X-ray source (ScientaOmicron GmbH). The analyzer pass energy of 20 eV gave an overall energy resolution (photons and spectrometer) of 0.35 eV. The binding energy scale was calibrated using the C 1s line at 284.6 eV as a reference. The data were analyzed using the CasaXPS software (N. Fairley, http://www.casaxps.com/) which employs a linear least squares optimization with a peak fitting algorithm including a Shirley background as part of the curve fitting process. A 30% Gaussian/70% Lorentzian peak shape was used.

For the TPD analysis, the samples were fixed on a stainless steel holder suspended in the center of a cylindrical quartz reactor by K-type thermocouple wires, 50 μm in diameter, spot-welded on the sample holder [5]. Heating (20 °C/min) was achieved by a (1.1 MHz, 6 kW) high-frequency system (EFD Induction S.A.) with an 6-turn inductive coil placed around the reactor. Analysis of species released during TPD runs was carried out by a quadrupole mass spectrometer (Thermo Smart-IQ$^+$). Prior to measurements, samples were annealed in the reactor to remove the contamination on the surface, checked for by quadrupole mass spectrometer indicating the CO$_2$ and H$_2$O signal above baseline level.

3. Results

The out of plane ($\theta - 2\theta$) XRD scans around the (002) reflection and around the (202) reflection for the 8, 15 and 30 nm thick films are shown
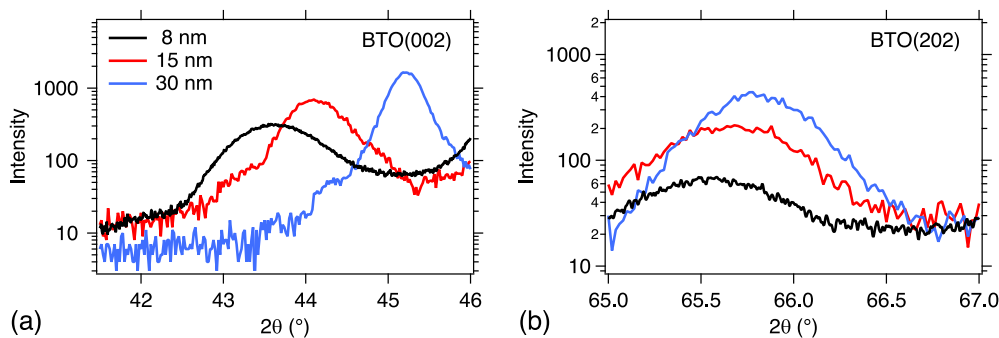
in Fig. 1(a) and (b). The out of plane scan intensities show a rising background with scattering angle due to the proximity of the intense (002) substrate peak. Nevertheless, the evolution in the lattice parameters with film thickness can be clearly observed. The in-plane a parameter is extracted from d$_{002}$ and d$_{202}$ values since the lattice is tetragonal.

The results are plotted in Fig. 1. Following Choi et al. the biaxial strain ϵ_s is defined as (a-a$_0$)/a$_0$ where a$_0$ is the lattice parameter in the unstrained bulk phase and a is the in-plane parameter of the strained film [6]. For the 8 nm film the in-plane lattice constant, a, is the same as that of the substrate (0.391 nm) indicating that the film is fully strained (2.2%) whereas the in-plane lattice constant for the 30 nm film is close to that of bulk BTO (0.400 nm) with a residual strain of only 0.2%. The out-of-plane tensile strain measured from the (001) peak and deduced assuming constant unit cell volume under strain is a maximum for the 8 nm and a minimum for the 30 nm film. These results are consistent with previous studies on epitaxial BTO films which start to relax above 8 nm when grown on SrTiO$_3$ [7].

Fig. 2 shows the c/a ratio or tetragonality. Tetragonality and hence out of plane strain are clearly anti-correlated to the film thickness. Higher strain means higher c/a ratio and therefore bigger ferroelectric distortion. Indeed high compressive strain favours strong out of plane polarization [8]. Choi report a remanent polarization of 50 μC/cm^2 for $\epsilon_s = -1.0\%$ and 70 μC/cm^2 for $\epsilon_s = -1.7\%$ [6]. However, as film thickness decreases the depolarizing field resulting from the out of plane polarization also increases and for very thin films can easily destabilize the ferroelectric state [9]. For the biaxial strains observed here, a critical thickness between 3 and 8 nm is expected. The films are therefore thicker than the critical thickness but lower out of plane film polarization might be expected due to the non-negligible depolarizing field [9].

On the other hand, following the model of Kim et al. [10] and based on the measured c/a ratios, the average film polarization in a capacitor geometry can be estimated to be 30, 40, 45 μC/cm^2 for the 8, 15 and 30 nm films, respectively, i.e. the polarization increases with film thickness. However, the model of Kim et al. is valid for polarization measurements
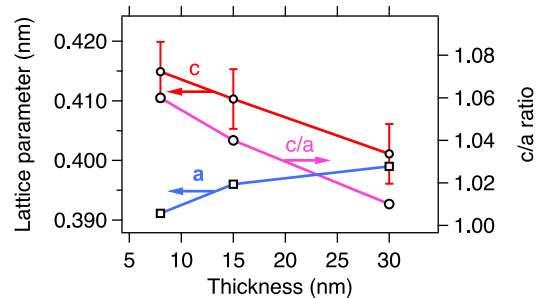
Fig. 2. Lattice parameters a (squares), c (small circles) and c/a (large circles) ratio as a function of thickness.

Fig. 1. θ-2θ XRD scans of BaTiO$_3$ (a) 002 reflection and (b) 202 reflection of 8 (black), 15 (red) and 30 (blue) nm films. (For interpretation of the references to color in this figure legend, the reader is referred to the web version of this article.)

in a capacitor geometry with strong screening by metallic electrodes. For our bare films, the effect of the depolarizing field could be much stronger and closer to the behavior described by Pertsev and Kohlstedt [9]. We have shown that in the absence of extrinsic screening such as that provided by a metallic electrode, the depolarizing field in ultra-thin films induces surface relaxation and the formation of a surface dipole opposite to the film polarization [3]. This provides an intrinsic screening mechanism and partially compensates the depolarizing allowing stabilization of the ferroelectric state. We conclude that the polarization of the thin film is correlated with strain, as suggested by Choi et al. [6], rather than thickness.

We have then investigated the chemistry of water adsorption as a function of strain. Sharp, (1×1) low energy electron diffraction patterns were obtained before and after water exposure, as shown in Fig. 3(a) and (b) indicating an unreconstructed surface with ordered, single monolayer adsorption on all three films.

Fig. 4 shows the XPS survey spectra for the 8, 15 and 30 nm films. The survey spectra are virtually identical and, importantly, the C 1s intensity is weak, close the XPS detection limit. We note that the C 1s core level, acquired with higher statistics and better resolution allow calibration of the binding energy scale as described in the experimental section. We conclude that the film surface are clean with a (1×1) reconstruction giving well-defined adsorption sites for water. The C 1s intensities (not shown) are less than 1% of the Ba 3d although the relative cross-section does imply a non-negligible surface carbon content. The 1s spectra have a main component due to adventitious C, and two weaker components typical of C–OH and carbonate bonding. The total C 1s intensity decreases by up to 25% for all three films after water exposure, due mainly to the attenuation of the main peak, which we ascribe to gradual desorption in UHV. The freeze-pump-thaw cycling has therefore introduced very little additional carbon. On the other hand, there is a slight increase in the C–OH intensity. C–OH bonding environment would typically be part of a larger entity such as CH_3–(CH)–OH. CH_3 fragments (15 amu) are characteristic of hydrocarbon thermal desorption, however, the signal at 15 amu is three orders of magnitude below that of water at 18 amu at all temperatures. We conclude that the thermally induced desorption of species including C–OH does not contribute to the 18 amu signal and that the latter is due to desorption from Ti and Ba.

Fig. 5 shows the Ba $3d_{5/2}$, Ti $2p_{3/2}$ and O 1s XPS core level spectra on the 8, 15 and 30-nm BTO films before (upper panels) and after (lower panels) exposure to water. The Ba $3d_{5/2}$ spectra have two components. The main peak, labeled I, is from the bulk-coordinated barium. Each spectrum also has a high binding energy (HBE) component labeled II, which is thought to be due to $Ba(OH)_2$ bonding in the near surface region [3]. The ratios of the Ba_{II}/Ba_I peak areas before and after water adsorption are given in Table 1.

The Ba_{II} increases by 1–2% of the overall 3d intensity on water adsorption. We suggest two possible routes for the formation of Ba–OH bonds. Firstly, the TiO_2-terminated surface is actually more open, less dense, than the BaO surface. As a result, the first BaO underlayer is exposed through the interstices of the TiO_2 surface [11]. Secondly, the films have terraces between 100 and 200 nm wide. The step edges therefore provide further Ba adsorption sites and the proportion of such
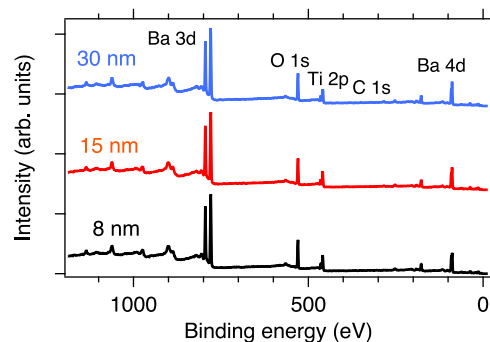

Fig. 4. XPS survey spectra for 8, 15 and 30 nm $BaTiO_3$ films. The level of carbon contamination is low, close to the XPS detection limit but still allows calibration of the binding energy scale.
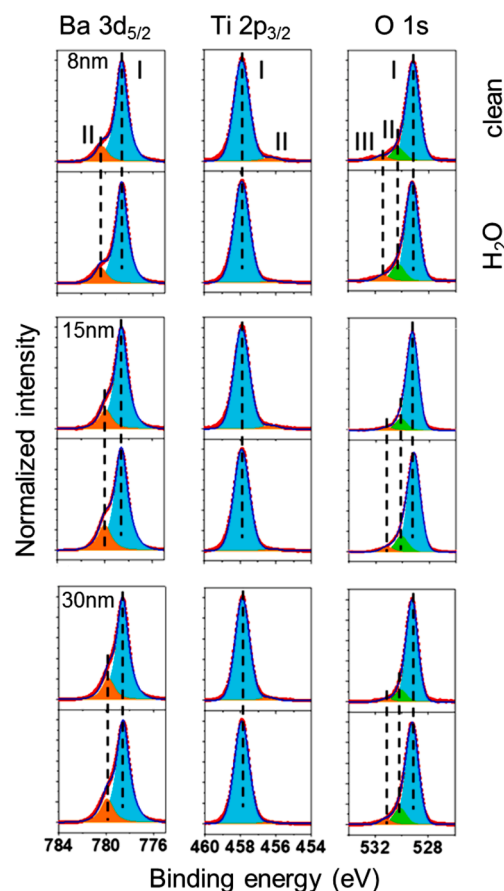

Fig. 5. XPS Ba 3d, Ti 2p and O 1s core level spectra on BTO thin film with different thickness before (top) and after (bottom) water exposure.

Table 1
Ba_{II}/Ba_I core level intensity ratios before and after water vapor adsorption for the three film thicknesses.

Thickness (nm)	Before	After
8	0.152	0.173
15	0.193	0.219
30	0.211	0.236

Fig. 3. Low energy electron diffraction image on 30-nm-thick BTO surfaces at 130 eV (a) before and (b) after water exposure.

sites is consistent with the increase in Ba_{II} intensity. Adsorption at step edges might even explain the Ba_{II} component before water adsorption since step edge migration is one way for layer-by-layer growth.
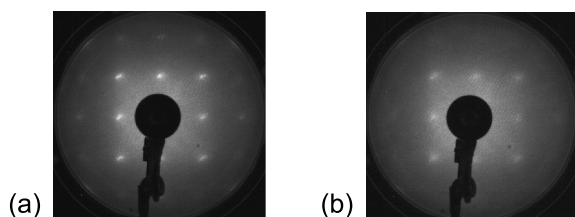
The O 1s spectra have three components, peak I has a BE of 529.1 eV, corresponding to oxygen in the bulk perovskite structure [12], as well as peaks II (BE 530.3 eV) and III (BE 531.6 eV), referred to as O_{II} and O_{III}. O_{II} component is due to a lattice oxygen coordinated with a proton and the O_{III} component is due to an OH^- group bonding [3]. The O_{II} can be due to H^+ bonding to a surface oxygen or to OH^- filling a surface V_O. In each case the intensity of the H^+ and OH^- related components increases after adsorption, as expected. The O 1s shift for molecular water is greater than 3 eV [13,14], thus, we do not think that O_{II} and O_{III} are due to molecular H_2O. The quantitative results for the O 1s spectra are reported in Table 2.

Finally, the three XPS spectra of Ti $2p_{3/2}$ before exposure to water have identical shapes with a main component due to Ti with a formal valency of 4+ as in the perovskite structure, and a weak, low binding energy (LBE) component corresponding to reduced Ti, often described as Ti^{3+}. The latter usually occurs due to charge transfer from a neighbouring oxygen vacancy, reducing two Ti^{4+} ions to Ti^{3+}. There are two energetically favorable sites for dissociative H_2O desorption, oxygen vacancy site and on-top surface Ti site [3]. Dissociation near an oxygen vacancy transfers a proton to an adjacent O atom, forming two OH^- pairs, one of which fills the V_O, the other appearing at an adjacent lattice oxygen site, reducing the Ti^{3+} intensity. Assuming that each oxygen vacancy is responsible for reducing two Ti^{4+} to Ti^{3+}, then water adsorption leads to a reduction in the V_O concentration of 0.16%, which is quite significant in terms of defect concentration but, nevertheless, difficult to detect in a change of the O 1s intensity. Both adsorption sites contribute to the O_{II} peak. On top bonding to surface Ti gives rise to four fold coordinated Ti and a proton bonding to a nearby lattice oxygen. 3.5% of the Ti ions are in the Ti^{3+} state for all films, decreasing to 2.5% after water adsorption. Mainly dissociative adsorption giving rise to OH^- groups bonding on-top to surface Ti atoms is predicted by theory [1] and corresponds to the O_{III} peak in the core level spectra. On the other hand, there is no significant difference in the Ti^{4+}/Ti^{3+} intensity ratio as a function of film thickness. Thus, strain does not change the preferred chemisorption sites or increase their number, but as will be seen it does influence the bond strength and adsorption energies, most likely due to strain induced atomic distortion and polarization.

We have used the core level intensities to calculate the near surface stoichiometry of the three films. Assuming a perfect TiO_2 surface termination, in the [001] direction the atomic layers alternate $TiO_2/BaO/TiO_2/$ The layer attenuation factor $k = \exp\{-c/(2\lambda)\}$, where c is the unit cell length along [001] and the values of the inelastic mean free path, λ are calculated from the NIST database, 0.83 nm, 1.1 nm and 1.04 nm for Ba, Ti and O, respectively. The total Ba, Ti and O intensities are then given by $I_{Ba}k/(1-k^2)$, $I_{Ti}/(1-k^2)$, $I_O(k+2)/(1-k^2)$, where $I_{Ba,Ti,O}$ are the Ba, Ti and O core level intensities expected from a single atomic layer [3]. The measured intensity is corrected by the relative cross-sections (O: 0.6036, 0.1069 and 0.04005 for Ba, Ti and O, respectively), and the stoichiometry deduced from $I_{Ba,Ti,O}$.

For the O 1s intensity we use $O_I + O_{II}$ since both are due to emission from oxygens in lattice sites. Setting the Ti stoichiometry to unity, we obtain $Ba_{1.001}TiO_{2.883}$ (8 nm), $Ba_{1.006}TiO_{2.891}$ (15 nm) and $Ba_{1.002}TiO_{2.904}$ (30 nm) before and $Ba_{1.002}TiO_{2.925}$ (8 nm), $Ba_{1.006}TiO_{2.943}$ (15 nm) and $Ba_{1.003}TiO_{2.943}$ (30 nm) after exposure to water. After growth the oxygen sub-stoichiometry is between 3.2 and

3.8%. Slight sub-stoichiometry is often observed for growth by molecular beam epitaxy.

Water exposure reduces the oxygen sub-stoichiometry to on average 2.1%. This implies a higher V_O concentration than that estimated from the intensity of the Ti^{3+} component in the Ti 2p spectra, indicating that both neutral and positively charged V_O are present but only the latter reduce Ti^{4+}. Importantly, despite slight variations in the sub-stoichiometry, the change in V_O as estimated from the Ti^{3+} intensity is the same after exposure to water. The surface chemistry is therefore the same for all three films and all are slightly Ba rich. We note that this is also consistent with the hypothesis of the formation of $Ba(OH)_2$ complexes in the near surface region.

The TPD spectra acquired from room temperature to 700 °C, using mass-to-charge ratio (m/e) = 18, are presented in Fig. 6. The relative intensities are directly related to the water desorption rate. Fig. 6(a) compares the TPD spectra of the 8, 15 and 30 nm films. The TPD data show a two stage water desorption process, one at low temperature (around 100–120 °C) and the second, more important stage with a strain dependent onset between 315 and 350 °C. This is clear evidence for the presence of dissociatively adsorbed water on the surface whereas the smaller proportion of physisorbed molecular water is desorbed at 100–120 °C [15,16]. Similar desorption features are observed for the three films except for a variation in the onset of the main peak. The onset of desorption peaks decreases from ∼ 350 °C on 8-nm-thick sample to ∼330 °C on 15-nm-thick sample, and finally ∼315 °C on 30-nm-thick sample, suggesting there is a systematic variation in E_{app} as a function of strain.

The mass spectrometry signals at 16, 17 and 18 mass to charge ratios (amu) were recorded simultaneously during TPD. They ratios are constant and correspond to H_2O fragmentation in the ion source of the MS. No predominant signal at 17 amu was observed which suggests that desorption of dissociated species is rapidly followed by recombination to give molecular water. Indeed, the recombination of adsorbed OH^- and H^+ to form water during the desorption process has been described on many surfaces [14,17,18].

The apparent activation energy of desorption can be calculated from a plot of ln p vs. 1/T of the desorption onset [5,19], where p is the partial pressure of the desorbed species and T the temperature, as presented in Fig. 6. The 8-nm-thick sample has the maximum slope, then the slope decreases on the 15-nm-thick sample, and is lowest for the 30-nm-thick sample. E_{app} is 1.28, 0.70 and 0.41 eV for 8, 15 and 30 nm films, respectively. The results are reported in Table 3 together with the biaxial strain deduced from XRD.

It is clear that the desorption energies vary with the strain, which also correspond to differences in film polarization [6,20]. The mechanism behind this effect can be considered from either an atomistic or a continuum perspective [21]. From the atomistic point of view, differences in the surface atomic structure of different strains must be considered. In order to stabilize polarization in the thin film, the first TiO_2 atomic layer corrugates and creates a dipole opposite to the bulk polarization to compensate the surface polarization charge [3]. It has been shown that the magnitude of the dipole varies with strain [22]. From the continuum perspective, the BTO thin films can be seen as polarized dielectric slabs in which the surface polarization charge may be screened by electrons and holes as well as surface specific atomic buckling. Thus, the electrostatic fields caused by different strains at the surface may influence the geometry and strength of adsorbate surface interactions and hence the screening of the surface polarization. The strain dependence of E_{app} is plotted in Fig. 7 and shows a linear relationship. As previously reported, OH^- on-top chemisorption at Ti site screens the surface charge better than rumpling of the dry surface [3] and has even been reported to be more efficient than metal electrodes [23]. We suggest that increased strain amplifies this effect giving rise to strain-dependent E_{app}.

Both atomic structure and surface electric fields certainly play a role

Table 2
O_{II}/O_I and O_{III}/O_I core level intensity ratios before and after water vapor adsorption for the three film thicknesses.

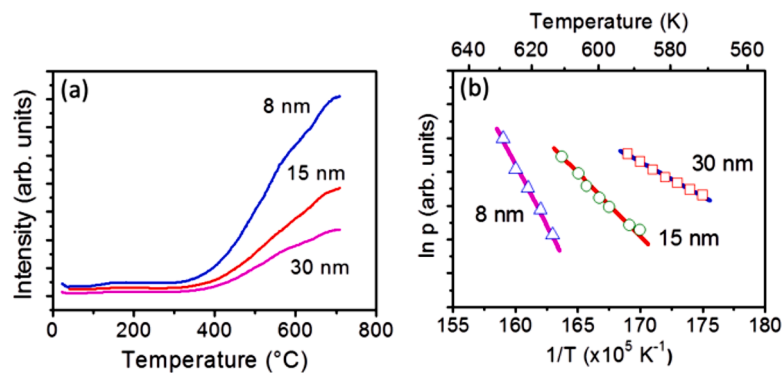| Thickness (nm)	Before		After	
	O_{II}/O_I	O_{III}/O_I	O_{II}/O_I	O_{III}/O_I
8	0.152	0.047	0.201	0.054
15	0.125	0.039	0.165	0.045
30	0.134	0.037	0.177	0.042

Fig. 6. TPD spectra on (a) BTO thin films with different thickness, and (b) Plot of ln p versus 1/T corresponding to the onsets of desorption at the low temperature tail of desorption spectra in (a).

Table 3
Bi-axial strain, ϵ_s (%), and apparent activation energy of desorption, E_{app} (eV), as a function of thickness (nm).

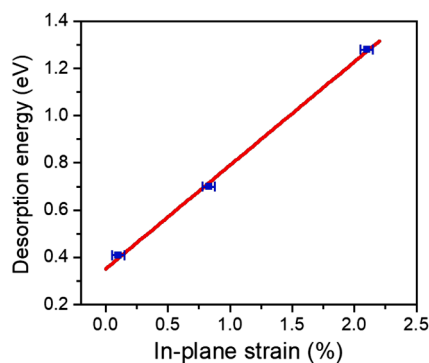| Thickness (nm)	ϵ_s (%)	E_{app} (eV)
8	2.2	1.28
15	0.9	0.70
30	0.2	0.41

Fig. 7. Desorption energy as a function of in-plane strain.

for the strain dependence of E_{app}. The efficient screening of the surface charge by OH^- bound to on-top surface Ti means that as strain and therefore ferroelectric distortion increases, E_{app} increases since the energy gain for the system is greater.

4. Conclusions

We have studied the adsorption and reaction of H_2O on TiO_2-terminated $BaTiO_3(001)$ surfaces with different strains by using X-ray diffraction, X-ray photoelectron spectroscopy and temperature-programmed desorption spectroscopy. The predominance of dissociative adsorption is supported by the two stage TPD spectra and the attenuation of the Ti^{3+} XPS component after water adsorption. The on-top OH^--Ti plays an important role in the chemisorption process. The apparent activation energy for water desorption decreases with the increasing of thickness, showing a strain-dependent chemisorption process. The dominant effect in determining E_{app} is the strain state of the film.

CRediT authorship contribution statement

J.L. Wang: Investigation, Writing - original draft. **S.J. She:** Investigation. **F. Gaillard:** Investigation, Writing - review & editing, Supervision. **G. Niu:** Investigation. **B. Vilquin:** Conceptualization, Investigation, Writing - review & editing. **N. Barrett:** Conceptualization, Investigation, Writing - review & editing, Supervision.

Declaration of Competing Interest

The authors declare that they have no known competing financial interests or personal relationships that could have appeared to influence the work reported in this paper.

Acknowledgments

References

[1] G. Geneste, B. Dkhil, Adsorption and dissociation of H_2O on in-plane-polarized $BaTiO_3(001)$ surfaces and their relation to ferroelectricity, Phys. Rev. B 79 (23) (2009) 235420, https://doi.org/10.1103/PhysRevB.79.235420.

[2] C. Park, D. Chadi, Effect of interstitial hydrogen impurities on ferroelectric polarization in $PbTiO_3$, Phys. Rev. Lett. 84 (20) (2000) 4717–4720.

[3] J.L. Wang, F. Gaillard, A. Pancotti, B. Gautier, G. Niu, B. Vilquin, V. Pillard, G.L.M. P. Rodrigues, N. Barrett, Chemistry and atomic distortion at the surface of an epitaxial $BaTiO_3$ thin film after dissociative adsorption of water, J. Phys. Chem. C 116 (41) (2012) 21802–21809, https://doi.org/10.1021/jp305826e.

[4] M. Kawasaki, T. Maeda, R. Tsuchiya, H. Koinuma, The $SrTiO_3$ crystal surface, Science 266 (1994) 1540–1542.

[5] F. Gaillard, J.P. Joly, A. Boréave, P. Vernoux, J.P. Deloume, Intermittent temperature-programmed desorption study of perovskites used for catalytic purposes, Appl. Surf. Sci. 253 (13 SPEC. ISS.) (2007) 5876–5881, https://doi.org/10.1016/j.apsusc.2006.12.054.

[6] K.J. Choi, M. Biegalski, Y.L. Li, A. Sharan, J. Schubert, R. Uecker, P. Reiche, Y. B. Chen, X.Q. Pan, V. Gopalan, L.-Q. Chen, D.G. Schlom, C.B. Eom, Enhancement of ferroelectricity in strained BaTiO3 thin films, Science 306 (5698) (2004), https://doi.org/10.1126/science.1103218.1005–9

[7] G. Niu, S. Yin, G. Saint-Girons, B. Gautier, P. Lecoeur, V. Pillard, G. Hollinger, B. Vilquin, Epitaxy of $BaTiO_3$ thin film on Si(001) using a $SrTiO_3$ buffer layer for non-volatile memory application, Microelectron. Eng. 88 (7) (2011) 1232–1235, https://doi.org/10.1016/j.mee.2011.03.028.

[8] N.A. Pertsev, A.G. Zembilgotov, A.K. Tagantsev, Effect of mechanical boundary conditions on phase diagrams of epitaxial ferroelectric thin films, Phys. Rev. Lett. 80 (9) (1998) 1988–1991, https://doi.org/10.1103/PhysRevLett.80.1988.

[9] N. Pertsev, H. Kohlstedt, Elastic stabilization of a single-domain ferroelectric state in nanoscale capacitors and tunnel junctions, Phys. Rev. Lett. 98 (25) (2007) 257603, https://doi.org/10.1103/PhysRevLett.98.257603.

[10] D. Kim, J. Jo, Y. Kim, Y. Chang, J. Lee, J.-G. Yoon, T. Song, T. Noh, Polarization relaxation induced by a depolarization field in ultrathin ferroelectric $BaTiO_3$ capacitors, Phys. Rev. Lett. 95 (23) (2005) 237602, https://doi.org/10.1103/PhysRevLett.95.237602.

[11] A. Berlich, H. Strauss, C. Langheinrich, A. Chassé, H. Morgner, Surface termination of $BaTiO_3(001)$ single crystals:A combined electron spectroscopic and theoretical

study, Surf. Sci. 605 (1-2) (2011) 158–165, https://doi.org/10.1016/j.susc.2010.10.014.

[12] J.D. Baniecki, M. Ishii, T. Shioga, K. Kurihara, S. Miyahara, Surface core-level shifts of strontium observed in photoemission of barium strontium titanate thin films, Appl. Phys. Lett. 89 (16) (2006) 162908, https://doi.org/10.1063/1.2357880.

[13] V.M. Fuenzalida, M.E. Pilleux, I. Eisele, Adsorbed water on hydrothermal BaTiO$_3$" lms: work function measurements, Vacuum 55 (1999) 81–83.

[14] I. Beinik, A. Bruix, Z. Li, K.C. Adamsen, S. Koust, B. Hammer, S. Wendt, J.V. Lauritsen, Water dissociation and hydroxyl ordering on anatase TiO$_2$ (001)-(14), Phys. Rev. Lett. 121 (20) (2018) 206003, https://doi.org/10.1103/PhysRevLett.121.206003.

[15] M. Shen, M.A. Henderson, Site competition during coadsorption of acetone with methanol and water on TiO$_2$(110), Langmuir 27 (15) (2011) 9430–9438, https://doi.org/10.1021/la2016726.

[16] J. Joly, F. Gaillard, E. Peillex, M. Romand, Temperature-programmed desorption (TPD) of water from iron, chromium, nickel and 304 L stainless steel, Vacuum 59 (4) (2000) 854–867, https://doi.org/10.1016/S0042-207X(00)00393-6.

[17] M.A. Henderson, S.A. Joyce, J.R. Rustad, Interaction of water with the (1 1) and (2 1) surfaces of α-Fe$_2$O$_3$(012), Surf. Sci. 417 (1) (1998) 66–81, https://doi.org/10.1016/S0039-6028(98)00662-1.

[18] T.F. Teng, W.L. Lee, Y.F. Chang, J.C. Jiang, J.H. Wang, W.H. Hung, Adsorption and thermal reactions of H$_2$O and H$_2$S on Ge(100), J. Phys. Chem. C 114 (2) (2010) 1019–1027, https://doi.org/10.1021/jp907791f.

[19] E. Habenschaden, J. Küppers, d ln (dn,,,/ dT), Surf. Sci. 138 (1984) L147.

[20] J.Y. Jo, Y.S. Kim, T.W. Noh, J.-G. Yoon, T.K. Song, Coercive fields in ultrathin BaTiO$_3$ capacitors, Appl. Phys. Lett. 89 (23) (2006) 232909, https://doi.org/10.1063/1.2402238.

[21] J. Garra, J. Vohs, D. Bonnell, The effect of ferroelectric polarization on the interaction of water and methanol with the surface of LiNbO$_3$(0001), Surf. Sci. 603 (8) (2009) 1106–1114, https://doi.org/10.1016/j.susc.2009.02.034.

[22] M. Fechner, S. Ostanin, I. Mertig, Effect of the surface polarization in polar perovskites studied from first principles, Phys. Rev. B 77 (9) (2008), https://doi.org/10.1103/PhysRevB.77.094112.

[23] J.E. Spanier, A.M. Kolpak, J.J. Urban, I. Grinberg, L. Ouyang, W.S. Yun, A.M. Rappe, H. Park, Ferroelectric phase transition in individual single-crystalline BaTiO$_3$ nanowires, Nano Lett. 6 (4) (2006), https://doi.org/10.1021/nl052538e.735–9